Solid-State Electronics 54 (2010) 143–148

Contents lists available at ScienceDirect

Solid-State Electronics

journal homepage: www.elsevier.com/locate/sse

# Electron subband structure in strained silicon UTB films from the Hensel–Hasegawa–Nakayama model – Part 2 efficient self-consistent numerical solution of the $\mathbf{k} \cdot \mathbf{p}$ schrödinger equation

Oskar Baumgartner *, Markus Karner, Viktor Sverdlov, Hans Kosina

*Institute for Microelectronics, TU Wien, Gußhausstraße 27–29, 1040 Wien, Austria*

ARTICLE INFO

*Article history:*
Received 24 April 2009
Received in revised form 10 June 2009
Accepted 2 September 2009
Available online 29 December 2009

The review of this paper was arranged by Prof. O. Engström

*Keywords:*
Two-band $\mathbf{k} \cdot \mathbf{p}$ model
Self-consistent solution
Numerical integration
Strained silicon
Two-dimensional electron gas
Ultra-thin body transistors

ABSTRACT

A self-consistent Schrödinger–Poisson model for the calculation of the electron subband structure of ultra-thin body (UTB) devices for arbitrary substrate orientation is presented. The proposed approach is based on a two-band $\mathbf{k} \cdot \mathbf{p}$ Hamiltonian and takes the band nonparabolicity and arbitrary strain into account. Despite its small matrix size compared to full-band approaches, an excellent description of the band structure over a wide range of the Brillouin zone is assured. Furthermore, emphasis is put on the efficiency and accuracy of the numerical, two-dimensional $\mathbf{k}$-space integration of the subband distribution functions. For this purpose, the Clenshaw–Curtis method which is based on non-equidistant interpolation nodes is employed. Simulation results of (0 0 1) and (1 1 0) oriented silicon UTB double gate devices demonstrate the suitability of the proposed numerical method. For Si body thicknesses in the nanometer regime, the presence of band structure effects which are not captured by a one-band model are clearly demonstrated.

© 2009 Elsevier Ltd. All rights reserved.

## 1. Introduction

The continuous progress in the development of semiconductor devices over the last decades has gone hand in hand with downscaling the device feature size [1]. For future CMOS technology nodes, strained silicon UTB MOSFETs are considered as good candidates. As the device feature sizes approach the wave length of free electrons quantum mechanical tunneling and energy quantization gain importance. The formation of subbands in the inversion channel of MOSFETs significantly affects the carrier transport. This is particularly true for UTB SOI devices, because the potential well is mainly determined by its geometrical structure. Fundamental carrier transport properties of MOS devices can be derived from one-dimensional vertical cuts through the channel. In that way quantum mechanical carrier confinement and electrostatic effects are captured. To solve the Schrödinger equation thereon, the conduction band in silicon is commonly approximated by three pairs of equivalent valleys located close to the *X*-points of the Brillouin zone. Near the minima the electron dispersion is well described by a one-band model. However, a recent study [2] showed the importance of effects that go beyond the possibilities of the parabolic band approximation (PBA) for modern UTB devices. An analytical approach to model these structures accurately has been presented in Part 1 [3]. While such analytical considerations are very useful to obtain a basic understanding of the problem, necessary assumptions like a square well potential pose a severe limitation to the model's applicability. Therefore, a more general numerical solution employing an efficient self-consistent Schrödinger model [4] is presented here. The implemented two-band $\mathbf{k} \cdot \mathbf{p}$ Hamiltonian is described in Section 2. A method to obtain the electron concentration by numerical integration of the occupied subbands is presented in Section 3 followed by a description of the simulation setup in Section 4. In Section 5 the effects of band nonparabolicity, arbitrary strain and crystal orientation on the electronic subband structure and effective masses are investigated and compared to full-band results.

## 2. Model Hamiltonian

The numerical modeling of the electron subband structure in UTB SOI MOS structures relies on an accurate description of the bulk Hamiltonian. In this work, we applied a two-band $\mathbf{k} \cdot \mathbf{p}$ Hamiltonian suggested by Hensel et al. [5,6] describing the silicon conduction band around the *X*-points.

* Corresponding author. Tel.: +43 1 58801 36015; fax: +43 1 58801 36099.
*E-mail address:* baumgartner@iue.tuwien.ac.at (O. Baumgartner).

0038-1101/$ - see front matter © 2009 Elsevier Ltd. All rights reserved.
doi:10.1016/j.sse.2009.12.010

$$\mathbf{H} = \begin{bmatrix} H_- & H_{\mathrm{bc}} \\ H_{\mathrm{bc}} & H_+ \end{bmatrix} \tag{1}$$

$$H_\mp = \mathscr{E}_{\mathrm{c}}(z) + \Xi_{\mathrm{u}}\varepsilon_{\ zz} + \frac{\hbar^2 k_z^2}{2m_{\mathrm{l}}} + \frac{\hbar^2\left(k_{\mathrm{x}}^2 + k_{\mathrm{y}}^2\right)}{2m_{\mathrm{t}}} \mp \frac{\hbar^2 k_0 k_z}{m_{\mathrm{l}}},$$

$$H_{\mathrm{bc}} = 2\Xi_{\mathrm{u}'}\varepsilon_{\mathrm{xy}} - \frac{\hbar^2 k_{\mathrm{x}} k_{\mathrm{y}}}{M}. \tag{2}$$

$\mathscr{E}_{\mathrm{c}}$ denotes the energy of the conduction band edge, $m_{\mathrm{l}}$ and $m_{\mathrm{t}}$ are the longitudinal and transversal electron masses, respectively, and $\frac{1}{M} \approx \frac{1}{m_{\mathrm{t}}} - \frac{1}{m_0}$ with the free electron mass $m_0$. A shear strain and a uniaxial deformation potential $\Xi_{\mathrm{u}'} = 7$ eV and $\Xi_{\mathrm{u}} = 9$ eV describe the effects of arbitrary strain on the band structure and $k_0 = 0.15\,\frac{2\pi}{a_0}$ corresponds to the distance of the valley from the $X$-point.

The quantization direction of the simulation system is assumed to be $\mathbf{e_z} = (0,0,1)^{\mathrm{T}}$. To account for arbitrary crystal orientations a rotation of the wave vector $\mathbf{k} \mapsto \mathbf{U_c k}$ with $\mathbf{k} = (k_{\mathrm{x}}, k_{\mathrm{y}}, k_{\ z})^{\mathrm{T}}$ is required. The unitary transformation matrix $\mathbf{U_c}$ is defined by the relation $\mathbf{e_z} = \mathbf{U_c}^{-1}\mathbf{e_n}$, where $\mathbf{e_n}$ is the quantization direction of the crystal coordinate system. Following the notation in the schematic Fig. 1, using the azimuthal and polar rotation angles $\varphi$ and $\vartheta$ the transformation from the crystal coordinate system to the simulation coordinate system can be written as

$$\mathbf{U_c} = \begin{bmatrix} \cos(\varphi)\cos(\vartheta) & -\sin(\varphi) & \cos(\varphi)\sin(\vartheta) \\ \sin(\varphi)\cos(\vartheta) & \cos(\varphi) & \cos(\varphi)\sin(\vartheta) \\ -\sin(\vartheta) & 0 & \cos(\vartheta) \end{bmatrix}.$$

Furthermore, the different valley orientations $v = \mathrm{x}, \mathrm{y}, \mathrm{z}$ need to be considered. Using the transformations

$$\mathbf{U_{v,x}} = \begin{bmatrix} 0 & 0 & -1 \\ 0 & 1 & 0 \\ 1 & 0 & 0 \end{bmatrix}, \quad \mathbf{U_{v,y}} = \begin{bmatrix} 0 & 0 & -1 \\ 1 & 0 & 0 \\ 0 & 1 & 0 \end{bmatrix}, \quad \mathbf{U_{v,z}} = \mathbf{I}$$

the total transformation matrix for valley $v$ and the crystal orientation is given by $\mathbf{U}_v = \mathbf{U_{v,v}U_c}$. To take strain into account for each valley type, the strain tensor is transformed by $\tilde{\varepsilon} \mapsto \mathbf{U_{v,v}}^{\mathrm{T}}\tilde{\varepsilon}\mathbf{U_{v,v}}$. Therefore, the diagonal blocks of the two-band $\mathbf{k}\cdot\mathbf{p}$ Hamiltonian (2) for arbitrary substrate orientation and valley sort $v$ are rewritten as

$$H_{\mp,v} = \mathscr{E}_{\mathrm{c}}(z) + \Xi_{\mathrm{u}}\varepsilon_{\mathrm{zz}} + \frac{\hbar^2}{2}\mathbf{k}^{\mathrm{T}}\mathbf{U}_v^{\mathrm{T}} \begin{bmatrix} \frac{1}{m_{\mathrm{t}}} & 0 & 0 \\ 0 & \frac{1}{m_{\mathrm{t}}} & 0 \\ 0 & 0 & \frac{1}{m_{\mathrm{l}}} \end{bmatrix} \mathbf{U}_v\mathbf{k} \mp \begin{bmatrix} 0 & 0 & \frac{\hbar^2 k_0}{m_{\mathrm{l}}} \end{bmatrix} \mathbf{U}_v\mathbf{k}.$$

The off-diagonal coupling components are substituted by the relation

$$H_{\mathrm{bc},v} = 2\Xi_{\mathrm{u}'}\varepsilon_{\mathrm{xy}} - \mathbf{k}^{\mathrm{T}}\mathbf{U}_v^{\mathrm{T}} \begin{bmatrix} 0 & \frac{\hbar^2}{M} & 0 \\ 0 & 0 & 0 \\ 0 & 0 & 0 \end{bmatrix} \mathbf{U}_v\mathbf{k}.$$

The quantization is introduced by the replacement $k_{\mathrm{z}} \to -\mathrm{i}\,\partial_{\mathrm{z}}$. The discretization is realized with a finite difference scheme with hard wall boundary conditions. The resulting eigenvalue problem gives rise to discrete energies describing the subband structure.

## 3. Numerical quadrature of subbands

The contribution of subband $\eta$ and valley $v$ to the equilibrium electron concentration is given by

$$n_{\eta,v}(z) = \frac{1}{(2\pi)^2}\int_{\mathrm{BZ}} \mathrm{d}^2\mathbf{k}\underbrace{|\psi_{\eta,v}(\mathbf{k},z)|^2 f_0(\mathscr{E}_{\eta,v}(k_{\mathrm{x}},k_{\mathrm{y}}) - \mathscr{E}_{\mathrm{F}})}_{f_{\eta,v}(\mathbf{k},z)}, \tag{3}$$

where $\psi_{\eta,v}$ is the normalized wave function and $f_0$ is the Fermi distribution function, $\mathscr{E}_{\mathrm{F}}$ denotes the Fermi level and $\mathscr{E}_{\eta,v}(k_{\mathrm{x}},k_{\mathrm{y}})$ the dispersion relation of the subband. Therefore, to calculate the electron occupation of a subband $\eta$ a numerical, two-dimensional $\mathbf{k}$-space integration is required. Hence, one seeks after a numerical quadrature scheme that gives good accuracy on a coarse grid. Contrary to previous work which made use of harmonic and cubic spline interpolation for $\mathbf{k}$-space integration [7], we applied the Clenshaw–Curtis method [8] for this purpose. In the integration interval $[-1,1]$ the zeros of the Chebyshev polynomial given by $x_k := \cos(k\frac{\pi}{N})$ with $k = 0,1,\ldots,N$ are used as nodes. The weights are written explicitly as [9]

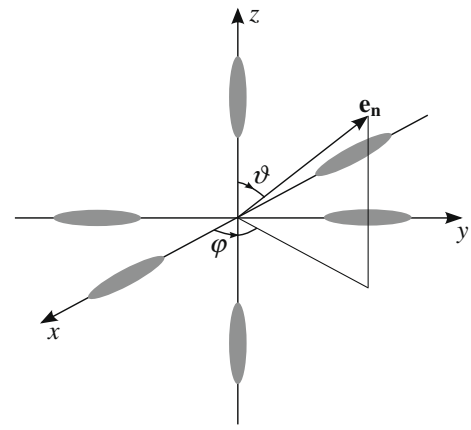


**Fig. 1.** Schematic of the silicon valleys around the $X$-point and their orientation. To describe arbitrary substrate orientations and all valley types, a rotation of the two-band $\mathbf{k}\cdot\mathbf{p}$ Hamiltonian is necessary. $\mathbf{e_n}$ is the normal unit vector to the substrate surface. $\varphi$ and $\vartheta$ are the azimuthal and polar angle from the simulation coordinate system to the crystal coordinate system.

$$w_k = \frac{c_k}{N}\left(1 - \sum_{j=1}^{\lfloor N/2 \rfloor} \frac{b_j}{4j^2 - 1}\cos\left(2jk\frac{\pi}{N}\right)\right)$$

with $b_j = 1$ if $j = N/2$, or $b_j = 2$ if $j < N/2$, and $c_k = 1$ if $k \bmod N = 0$, or $c_k = 2$ otherwise. An advantage of this method is the ability to use subsets of half the number of the nodes for a lower degree rule. This allows for adaptive numerical quadrature schemes which have proven suitable for energy domain integration as shown for the NEGF method in [10]. Furthermore, the accuracy of the numerical quadrature can be checked by comparing the integral of a higher and a lower order rule. The two-dimensional integration is carried out by repeated one-dimensional integration of $f_{\eta,v}(k_{\mathrm{x}},\ k_{\mathrm{y}},z)$ (cf. (3)).

$$n_{\eta,v}(z) = \frac{1}{(2\pi)^2}\int_{k_{\mathrm{x,min}}}^{k_{\ \mathrm{x,max}}}\left(\int_{k_{\mathrm{y,min}}}^{k_{\mathrm{y,max}}} f_{\eta,v}(k_{\ \mathrm{x}},k_{\mathrm{y}},z)\mathrm{d}k_{\mathrm{y}}\right)\mathrm{d}k_{\mathrm{x}}$$

For the $\mathbf{k}$-space integration of the subbands provided by the two-band Hamiltonian excellent accuracy has been achieved with only 19 nodes per $k$ direction.

## 4. Simulation setup

To properly incorporate the electrostatics in realistic devices a self-consistent Schrödinger–Poisson scheme has been employed. The electron concentration in the quantized well is calculated by using (3) with the dispersion relation obtained by (2). The carrier concentration in the gate regions is calculated classically. The hereby obtained charge density is used as input for the Poisson equation and the procedure is iterated until convergence is achieved. As test device a silicon ultra-thin body double gate nMOSFET with 3 nm film thickness and 1 nm oxide thickness has been simulated. The donor doping of the polysilicon gates was

$N_D = 1.0 \times 10^{20}$ cm$^{-3}$ and the Si film was lightly p-doped at $N_A = 2.0 \times 10^{16}$ cm$^{-3}$.

## 5. Results and discussion

The ultra-thin body DG-nMOS device has been simulated using two different substrate orientations. The self-consistent results for (0 0 1) and (1 1 0) substrates are presented in the following sections.

### 5.1. Substrate orientation (0 0 1)

Fig. 2 shows the numerically calculated dispersion relation of the first and second unprimed subband of the UTB device. The contour plots illustrate the ellipsoidal deformation of the subband structure caused by shear strain. The results are in good agreement with analytical considerations [11].

The occupied subbands are illustrated in Fig. 3 for zero gate voltage. The origin of the plots corresponds to the *X*-point. The left and the middle figure show the first and second unprimed subband, respectively. On the right side the first primed subband is given. The superimposed grid corresponds to the nodes of the Clenshaw–Curtis quadrature. The method results in an accumulation of grid points at the boundary of the integration domain.

The application of $\varepsilon_{xy} = 0.5\%$ shear strain leads to an deformation of the electronic subband structure. Fig. 4 shows the effect on the occupied subbands. The numerical integration routine is able to handle such different integrand shapes and the self-consistent Schrödinger/Poisson scheme typically converges within ten iterations.

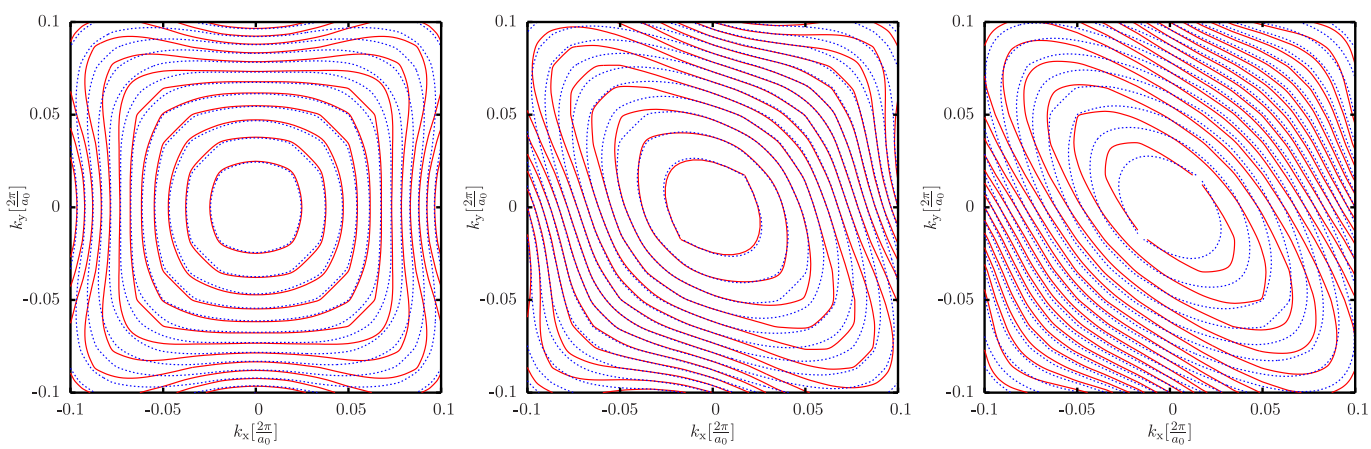


**Fig. 2.** Dispersion relation of the first (solid line) and second (dashed line) unprimed subband of a 3 nm wide, (0 0 1) silicon quantum well for different values of shear strain (from left to right $\varepsilon_{xy} = 0.0\%$, $\varepsilon_{xy} = 0.5\%$, and $\varepsilon_{xy} = 1.0\%$). The contours are stepped in 20 meV intervals.

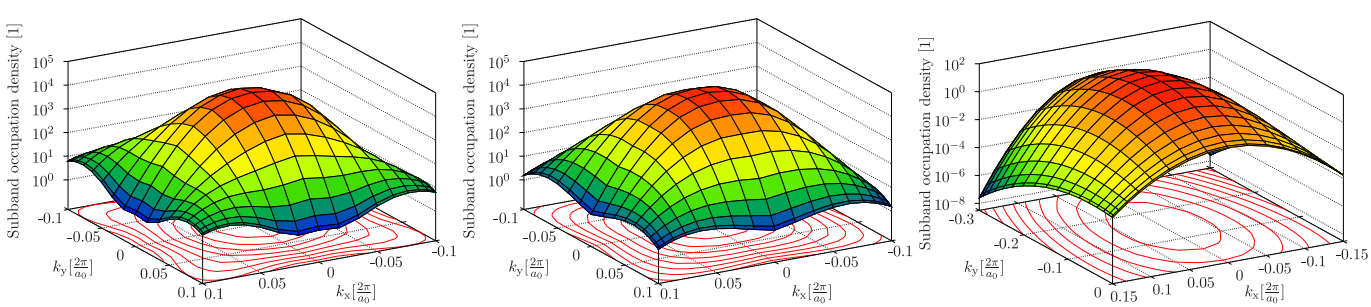


**Fig. 3.** Occupation of the first and second unprimed subband and the first primed subband of a 3 nm wide silicon quantum well. The gate voltage of the DG-nMOSFET is 0 V. The grid corresponds to the nodes of the numerical quadrature.

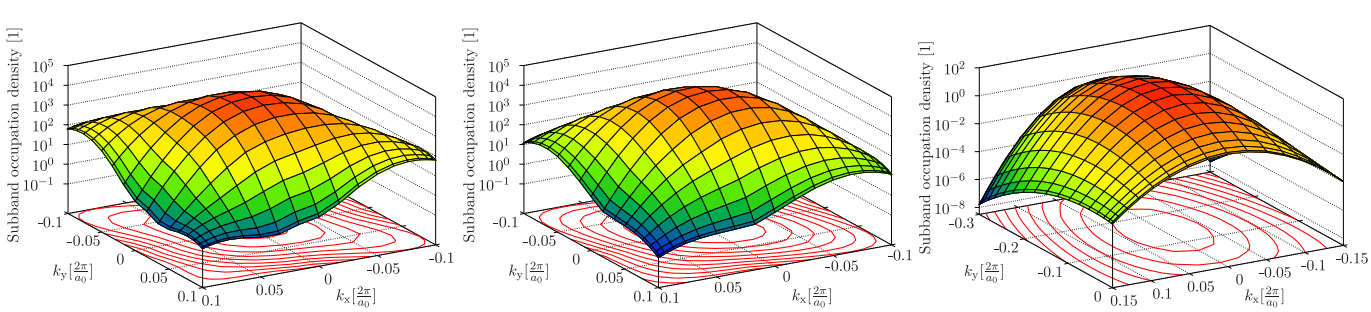


**Fig. 4.** Similar to Fig. 3 but with shear strain $\varepsilon_{xy} = 0.5\%$. The unprimed subbands are deformed and shifted downwards with respect to the primed subband. The primed subband is not affected by shear strain.

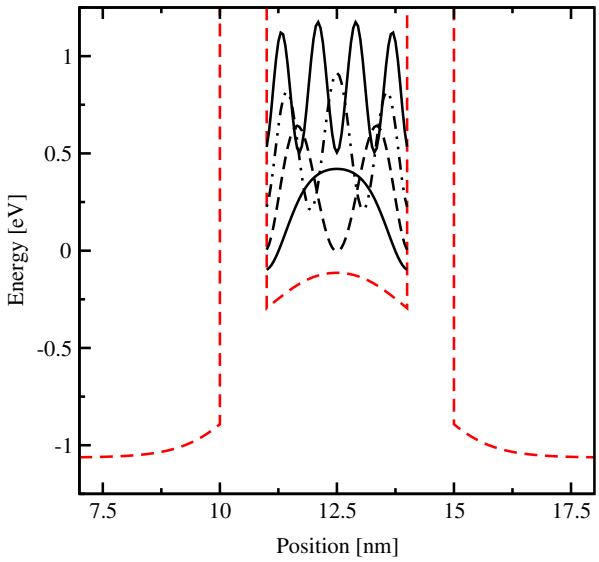


**Fig. 5.** Self-consistent calculation of the conduction band edge of a (001) Si-DG-nMOSFET with 3 nm well width and 1 nm oxide thickness. The normalized wave functions ($nm^{-1}$) are overlayed at their respective energy levels.

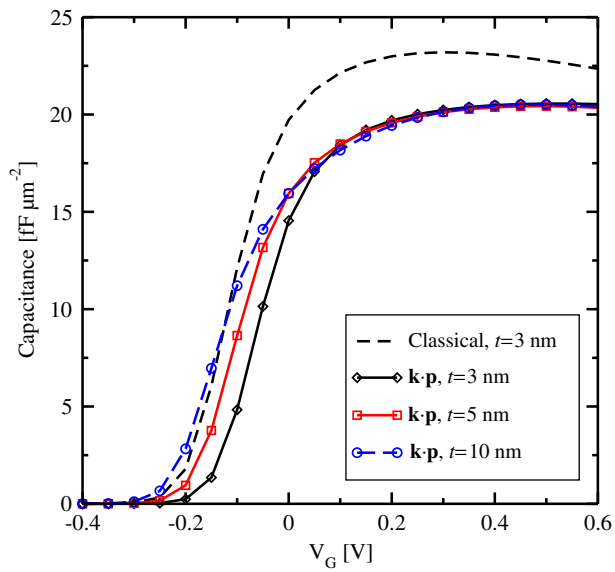


**Fig. 7.** Capacitance versus gate voltage for different film thicknesses $t$ of the (001) silicon UTB DG-MOS device.

As a result of this self-consistent simulation, the carrier concentration and the conduction band edge are obtained. Fig. 5 shows the conduction band edge provided by the converged iteration scheme. Within the well the squared wave functions for the four lowest, twofold degenerate unprimed subbands are displayed at their corresponding energy levels.

For each of these subbands the electron occupation is calculated by **k**-space integration. The resulting carrier concentration within the well is depicted in Fig. 6. For comparison, the classically calculated results are included. As shown, the difference in the total electron concentration because of shear strain is more pronounced at a lower gate bias voltage. The CV characteristics of the device are given in Fig. 7. The charge is calculated by summing up the charge density in the polysilicon gate region. The classically obtained result is included for comparison and illustrates its overestimation of carriers within the well region. Additionally, the well width $t$ of the (001) silicon UTB DG-MOS device has been varied. As expected, a thinner film leads to an increased threshold voltage. The simulations have been repeated with shear strain of $\varepsilon_{xy} = 0.5\%$ and results are shown in Fig. 8. Since strain moves the unprimed subband ladder down in energy, the subbands are, therefore, already occupied at lower bias. This effectively shifts the whole capacitance-voltage characteristics to lower gate voltages.

### 5.2. Substrate orientation (110)

A (110) silicon ultra-thin body nMOSFET with 1 nm oxide thickness and varying film thickness has been simulated. Contour

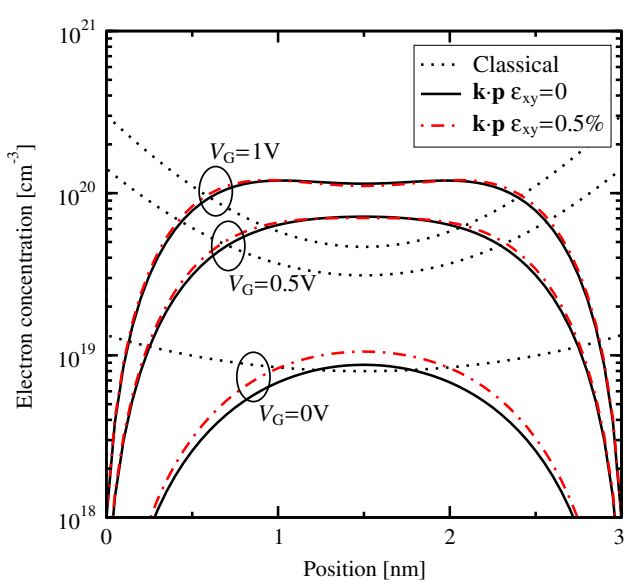


**Fig. 6.** Self-consistent calculation of the electron concentration of a (001) Si-DG-nMOSFET with 3 nm film thickness. The effect of shear strain $\varepsilon_{xy} = 0.5\%$ on the electron concentration is illustrated for various gate bias.

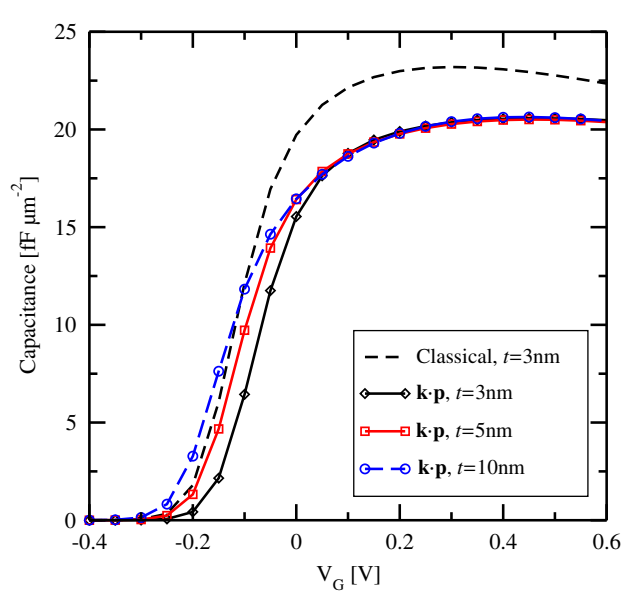


**Fig. 8.** Similar to Fig. 7 but with shear strain of $\varepsilon_{xy} = 0.5\%$. Due to strain, the characteristics are shifted slightly to lower gate voltages.

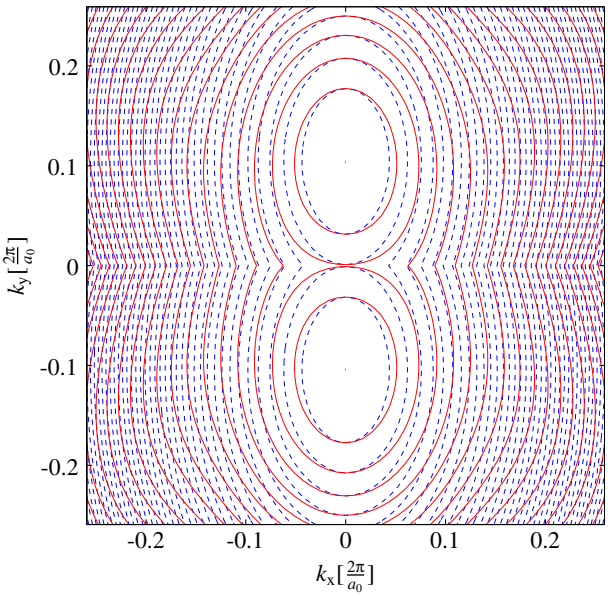


**Fig. 9.** Dispersion of the unprimed subband around the *X*-point for the two-band $\mathbf{k}\cdot\mathbf{p}$ method and with PBA (dashed line) for a film thickness of $t = 3$ nm.

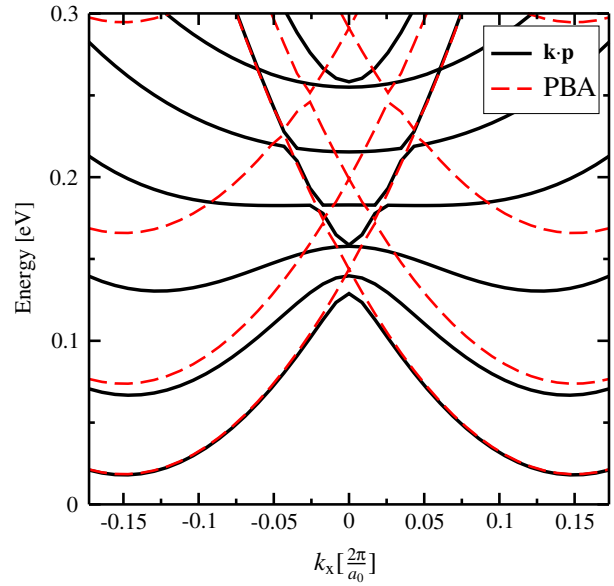


**Fig. 11.** Dispersion of the primed subbands around the *X*-point for the two-band $\mathbf{k}\cdot\mathbf{p}$ method and with PBA (dashed line) for a film thickness of $t = 10$ nm. In the nonparabolic case, the subbands are split at the *X*-point.

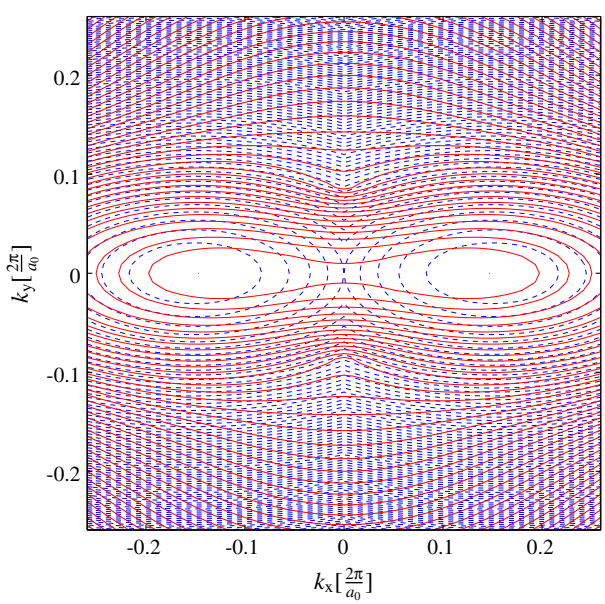


**Fig. 10.** Dispersion of the primed subband around the *X*-point for the two-band $\mathbf{k}\cdot\mathbf{p}$ method and with PBA (dashed line) for a film thickness of $t = 3$ nm. The valley is shifted towards the *X*-point in the nonparabolic case.

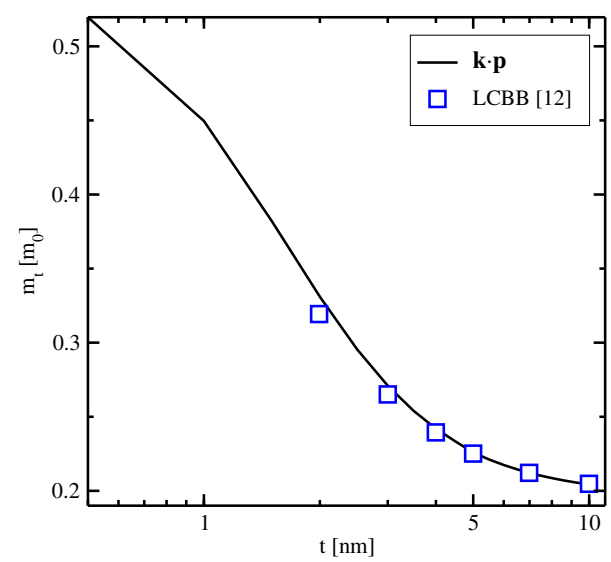


**Fig. 12.** Transverse effective masses of the first unprimed valley of a (1 1 0) Si thin film extracted from the two-band $\mathbf{k}\cdot\mathbf{p}$ method compared to full-band results calculated with the local combination of bulk bands method [12].

plots of the dispersion relations for a film thickness of $t = 3$ nm are depicted in Figs. 9 and 10 for the lowest unprimed and primed subband, respectively. The minimum of the primed valley moves towards the *X*-point with decreasing film thickness, which can not be seen with the parabolic band approximation. The dispersion of the first and second primed subband calculated by the two-band $\mathbf{k}\cdot\mathbf{p}$ method shows a splitting at the *X*-point even without strain, whereas parabolic bands cross (Fig. 11).

The transverse masses of a (1 1 0) Si thin film have been extracted by fitting a parabola near the valley minimum. Fig. 12 gives the transverse effective masses in [0 0 1] direction of the unprimed valley as a function of the UTB well width. The two-band $\mathbf{k}\cdot\mathbf{p}$ results are compared to full-band calculations provided by the linear combination of bulk bands (LCBB) method and show excellent agreement with the values of [12]. Fig. 13 depicts the decrease of the transverse mass in $[\bar{1}\,1\,0]$ direction of the primed subband by reducing the film thickness. The application of 1 GPa tensile stress in $[\bar{1}\,1\,0]$ direction greatly enhances the the effect of mass reduction, as shown for the first primed subband. Likewise, the energy levels of the valleys depend on film thickness. Fig. 14 shows the lowest primed and unprimed subband energies. One gigapascal tensile stress in $[\bar{1}10]$ is applied to shift the primed subband down in energy and thereby attain a redistribution of electrons by decreasing the occupation of the unprimed subbands. As shown, the primed subband moves significantly below the unprimed subband. Thereby, tensile stress simultaneously reduces the transport mass of the primed valley and increases their occupation leading to mobility and current enhancement in $[\bar{1}\,1\,0]$ direction.

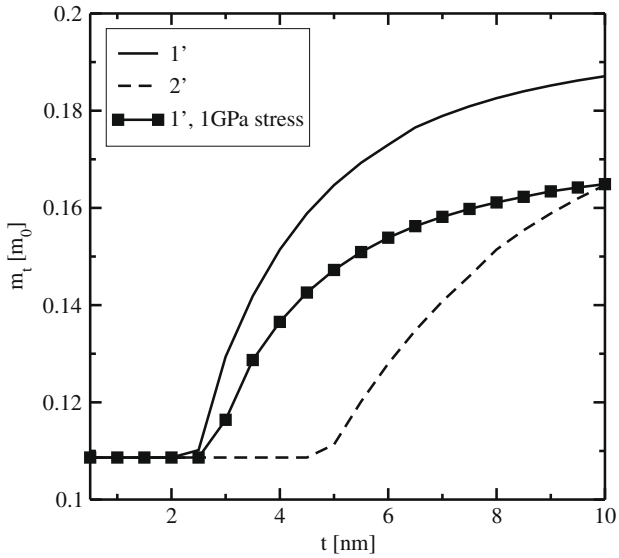


**Fig. 13.** Transverse effective masses of the primed ladder of a (1 1 0) Si thin film extracted from the two-band $\mathbf{k}\cdot\mathbf{p}$ method. By applying 1 GPa tensile stress in [$\bar{1}$10] the mass is reduced further.

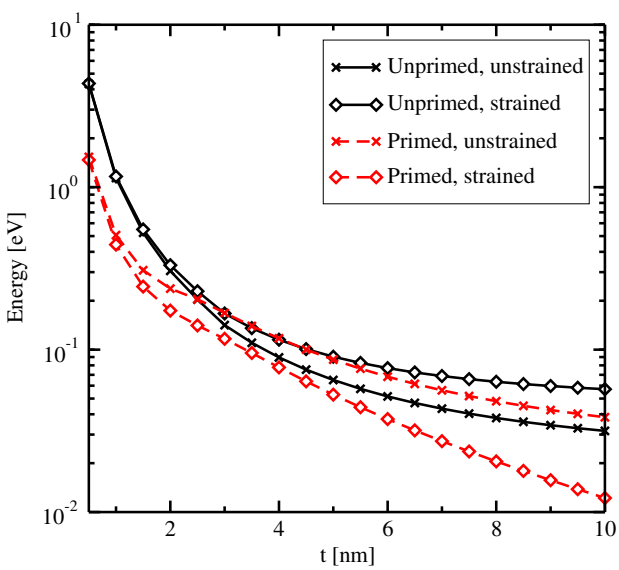


**Fig. 14.** Subband levels of a (1 1 0) Si thin film. One gigapascal tensile stress in ($\bar{1}$ 1 0) alternates the order of the unprimed and primed subbands.

## 6. Summary and conclusion

An accurate self-consistent two-band $\mathbf{k}\cdot\mathbf{p}$ Schrödinger–Poisson model, which describes the electronic subband structure for arbitrary quantization directions has been implemented. Only one additional parameter $M$ characterizing the band coupling is introduced. The Clenshaw–Curtis method is employed for the 2D **k**-space integration of the subbands. The carrier concentration and the conduction band edge are calculated in a self-consistent iteration scheme. The effects of strain and band nonparabolicity are accounted for. Numerical results for (0 0 1) and (1 1 0) Si UTB devices are investigated. In ultra-thin films quantization and band coupling lead to a substantial deformation of the subbands which is not covered by the parabolic band approximation: in (0 0 1) substrates the effects of nonparabolicity on the subband dispersion are illustrated. For (1 1 0) silicon a shift of the primed valley minimum towards the $X$-point is observed, which affects the energy difference to the unprimed ladder. Furthermore, tensile stress in [$\bar{1}$ 1 0] moves the primed subbands below the level of the unprimed subbands.

## Acknowledgment

This work has been supported in part by the Austrian Science Fund, special research program IR-ON (F2509).

## References

[1] International technology roadmap for semiconductors. <http://www.itrs.net>.
[2] Uchida K, Kinoshita A, Saitoh M. Carrier transport in (1 1 0) nMOSFETs: subband structures, non-parabolicity, mobility characteristics, and uniaxial stress engineering. In: IEDM Techn Dig; 2006. p. 1–3.
[3] Windbacher T, Sverdlov V, Baumgartner O, Selberherr S. Electron subband structure in strained silicon UTB films from the Hensel–Hasegawa–Nakayama model – part 1 analytical consideration and strain-induced valley splitting. Solid-State Electron 2010;54(2):137–42.
[4] Baumgartner O, Karner M, Sverdlov V, Kosina H. Numerical study of the electron subband structure in strained silicon UTB devices. In: EUROSOI 2009 conference proceedings; 2009. p. 57–8.
[5] Hensel JC, Hasegawa H, Nakayama M. Cyclotron resonance in uniaxially stressed silicon. II. Nature of the covalent bond. Phys Rev 1965;138(1A): A225–38.
[6] Ungersböck E, Dhar S, Karlowatz G, Sverdlov V, Kosina H, Selberherr S. The effect of general strain on the band structure and electron mobility of silicon. IEEE Trans Electron Dev 2007;54(9):2183–90.
[7] Pham A-T, Meinerzhagen B, Jungemann C. A fast $\mathbf{k}\cdot\mathbf{p}$ solver for hole inversion layers with an efficient 2D $k$-space discretization. J Comp Electron 2008;7(3):99–102.
[8] Clenshaw CW, Curtis AR. A method for numerical integration on an automatic computer. Numer Math 1960;2:197–205.
[9] Waldvogel Jörg. Fast construction of the Fejér and Clenshaw–Curtis quadrature rules. BIT 2006;46:195–202.
[10] Baumgartner O, Karner M, Holzer S, Pourfath M, Grasser T, Kosina H. Adaptive energy integration of non-equilibrium Green's function. In: Proceedings of the 2007 NSTI nanotechnology conference, vol. 3; 2007. p. 145–8.
[11] Sverdlov V, Karlowatz G, Dhar S, Kosina H, Selberherr S. Two-band $\mathbf{k}\cdot\mathbf{p}$ model for the conduction band in silicon: impact of strain and confinement on band structure and mobility. Solid-State Electron 2008;52(10):1563–8.
[12] van der Steen J-L, Esseni D, Palestri P, Selmi L, Hueting R. Validity of the parabolic effective mass approximation in silicon and germanium n-MOSFETs with different crystal orientations. IEEE Trans Electron Dev 2007;54(8): 1843–51.